Article

Manganese cobalt-based spinel coatings processed by electrophoretic deposition method: the influence of sintering on degradation issues of Solid Oxide Cell oxygen electrodes at 750 °C

Elisa Zanchi [1], Justyna Ignaczak [2], Bartosz Kamecki [2,3], Piotr Jasiński [2], Sebastian Molin [2], Aldo R. Boccaccini [4], Federico Smeacetto [1]*

[1] Department of Applied Science and Technology, Politecnico di Torino, Corso Duca degli Abruzzi 24, 10129 Torino, Italy
[2] Advanced Materials Centre, Faculty of Electronics, Telecommunications and Informatics, Gdańsk University of Technology, ul. G. Narutowicza 11/12, 80-233 Gdańsk, Poland;
[3] Advanced Materials Centre, Faculty of Applied Physics and Mathematics, Gdańsk University of Technology, ul. G. Narutowicza 11/12, 80-233 Gdańsk, Poland;
[4] Department of Materials Science and Engineering, University of Erlangen-Nuremberg, Cauerstr. 6, 91058 Erlangen, Germany

* Correspondence: federico.smeacetto@polito.it;

Abstract: This paper seeks to examine how the Mn-Co spinel interconnect coating microstructure can influence the Cr contamination in an oxygen electrode of intermediate temperature Solid Oxide Cells at the operating temperature of 750 °C. A Mn-Co spinel coating is processed on Crofer 22 APU substrates by electrophoretic deposition and subsequently sintered following both the one-step and two-step sintering, in order to obtain significantly different densification levels. The electrochemical characterization is performed on anode supported cells with a LSCF cathode. The cells were aged prior to the electrochemical characterization in contact with the spinel coated Crofer 22 APU at 750 °C for 250 hours. Current-voltage and impedance spectra of the cells were measured after the exposure with the interconnect. Post-mortem analysis of the interconnect and the cell was carried out in order to assess the Cr retention capability of coatings with different microstructures.

Keywords: electrophoretic deposition; manganese cobalt spinel; Solid Oxide Cell; chromium poisoning

1. Introduction

Volatile Cr species released from steel interconnects of Solid Oxide Cell (SOC) stack at different oxygen partial pressures migrate and deposit on the air electrode, thus leading to a substantial and fast degradation of the electrochemical performance of the SOC cells. The outward Cr migration is partially limited by introducing ~0,5 wt.% of Mn in the Crofer 22 APU alloy; anyway, the Cr–Mn spinel that develops at the top of the chromia scale has been reported to partially limit, but not completely avoid the oxygen electrode degradation [1]. The application of a ceramic protective coating on steel interconnects of SOC stacks is a widely employed solution to limit the steel oxidation rate and chromium evaporation [2]. In principle, two main factors influence the protective performance of such coatings: chemical composition and densification. Among various proposed materials in the spinel family, perovskites and rare earth oxides, manganese cobalt spinel coatings have shown a good balance in terms of chromium blocking capability, matched thermal expansion coefficient and high electrical conductivity at the SOC operating temperatures (500-850 °C) [3,4]. In recent years, research has been focusing on the implementation of the electrical and thermochemical properties of the base Mn-Co spinel by transition metals doping (mainly Cu, Fe and Ni) [5–7] or rare earth elements modification [8–10]. Different deposition methods have been reported in literature for Mn-Co spinel coatings. For example, sputtering [11,12], electroplating [13] and plasma spray [14] allow to obtain highly

dense coatings and a sintering treatment may not be required. On the other hand, when screen printing [15,16] or slurry based methods like deep coating [17,18] and electrophoretic deposition (EPD) [19–21] are used, a post-deposition treatment is always required in order to consolidate and densify the deposited powders and reduce the residual porosity. EPD is a fast and versatile process which allows to deposit homogeneous layers in few seconds and at RT condition on complexly shaped steel components [22–24]. Furthermore, EPD offers the possibility to tune the spinel composition "in-situ", by co-depositing the base spinel together with desired amounts of Fe_2O_3 [25,26] or CuO [7,27], in order to obtain respectively iron or copper doped and modified manganese cobalt spinel coatings. In a recently published article by Sabato et al. [28], EPD was proved to be an optimal deposition method to coat real dimension SOFC interconnects: despite the numerous corrugated and channeled surfaces on the Crofer 22 APU interconnect, the EPD deposited Mn-Co spinel-based coating showed great stability and maintained protective properties after the stack test at 850°C.

The coating deposition method and the consequent sintering profile are critical in obtaining well performing protective coatings. Sintered coatings should be dense in order to limit possible chromium evaporation and gas access to the oxide scale. A certain degree of porosity can be however considered beneficial, as this might stop possible cracks from propagating further. Although a two-step sintering, consisting of a reduction followed by a re-oxidation step, is widely recognized as a valid post-deposition treatment to achieve high coating densification, it causes the increase of the processing cost of the interconnect [20,29]. Indeed, even poorly densified spinel coatings subjected to the one-step sintering in air only could ensure sufficient protection against Cr vaporization and corrosion of the interconnect during the stack operation at 800 °C [30]**.** In a previous study, Molin et al. [12] showed that the manganese cobalt spinel coating deposited by EPD and submitted to the one step sintering (oxidation) in static air reduced the oxide scale growth rate during the 5000 h tests at 800 °C, presenting the best protection in comparison to manganese cobalt spinel processed by physical vapour deposition methods. The study demonstrated the efficacy of a single step sintering (thus excluding the reduction heat treatment step) in an effort to reduce the overall coating processing cost. This long-term study was focused on the area specific resistance (ASR) degradation rate, while no indication of Cr poisoning of the cathode was reported. Moreover, with lower temperature as in IT-SOC, the relative importance of Cr evaporation compared to the oxide scale growth becomes larger [31]. The present study investigates the effect of coating density on cell performance and cathode poisoning at the operating temperature of 750 °C. To this purpose, a $Mn_{1.5}Co_{1.5}O_4$ spinel coating was deposited on Crofer 22 APU substrates by electrophoretic method. As deposited samples were then sintered following the one-step or two-step sintering processes, in order to obtain significantly different densification levels. Since the sintering procedure can play an important role in addressing the issue of preventing Cr evaporation, the final aim of this work is to evaluate the convenience of performing a two-step sintering process on the cell degradation rate for IT-SOC stacks. The results that are presented here show how different densification levels of spinel-based coatings can play a critical role on reactivity with chromium, examining the relationship between the whole sintering procedure and the required manganese cobalt coating performance.

2. Materials and Methods

2.1 Coating deposition and sintering

Steel coupons with the size of 15×15 mm^2 were cut from a 0.3 mm thick plate of Crofer 22 APU (Cr=23 wt.%, Mn=0.45 wt.%, La=0.1 wt.%, Ti=0.06 wt.%, Si and Al<0.05 wt.%, Fe=Bal.) provided by VDM Metals (Verdohl, Germany). The coupons were cleaned in acetone and ethanol for 10 min each in ultrasonic bath prior to deposition. The EPD suspension consisted of a mixture of ethanol and deionized water (60/40 vol.%) to which manganese-cobalt spinel powder with a chemical composition of $Mn_{1.5}Co_{1.5}O_4$ (Fuelcellmaterials, d50 =0.6 μm) was added to reach a solid content of 37.5 g/l. More details about the

preparation of the suspension can be found in a previous work [32]. In order to coat both surfaces of the samples, electrophoretic deposition was performed in a three-electrode setup already described in [25], applying 50 V for 20 s and with a sample-electrode distance of 1 cm. After drying, the coated coupons were heat treated following two separate procedures. A first batch of samples was subjected to a one-step sintering (oxidation only) at 900 °C for 2 h in static air: these samples are labeled 20s_Ox. On the other hand, the second set of samples were exposed to a two-step sintering, consisting a first heat treatment at 1000 °C for 2 h in flowing Ar/H_2 5%, gas (reduction) and subsequently a second treatment at 900 °C for 2 h in static air (re-oxidation). These samples are therefore referred as 20s_RedOx. Few samples were not subjected to the re-oxidation step to conduct morphological and compositional analysis of the coating after the reduction; these samples are labeled as 20s_Red.

2.2. Area Specific Resistance measurement test

To examine the effect of the two sintering methods on the electrical properties, ASR measurements on the as-prepared 20s_Ox and 20s_RedOx coatings were performed. Platinum electrodes were painted (ESL 5542 conductive paste, ESL, Reading, UK) on both sides of the spinel coated samples to form symmetrical electrodes in a cross-scale measurement configuration. The solvent from the paste was evaporated at 100 °C on a hot plate and then the samples were heated up to 750 °C for 10 minutes. The measurement was carried out in a four-electrode system with 5 mV sinusoidal amplitude of 1 Hz (Gamry Interface 1000 Potentiostat/Galvanostat/ZRA, Warminster, USA). The sample was heated up to 750 °C, and then cooled to 200 °C with simultaneous impedance measurements. The ASR value of the samples was calculated taking into account the electrode area and divided by two to obtain a value for a single interface.

2.3 Interconnect aging, Cr evaporation exposure and fuel cell test

To evaluate the protective properties of the prepared coatings, aging test was performed. Anode Supported Solid Oxide Fuel Cells (ASC-SOFC, produced by TaipeiTech, Taipei, Taiwan) were used for the test. The 2.54 cm diameter cells were prepared by tape-casting/screen printing processes. Structure of the cell consisted of Ni-YSZ porous support, Ni-YSZ active electrode, 25 μm thick YSZ electrolyte, 8 μm thick CGO diffusion barrier layer, and 30 μm thick LSCF oxygen electrode with 1 cm^2 active surface area. The cells have been exposed in the presence of differently coated steel interconnects in tube furnace, according to a procedure similar to the one reported in [21]. For cell performance evaluation three cells were aged: a reference cell without any steel placed onto the oxygen electrode, and two cells with coated steel described as 20s_Ox and 20s_RedOx, respectively. Each cell was aged separately to avoid possible Cr evaporation from the steel and poisoning mutually. The test was performed in a continuous flow of humidified atmospheric air for 250 h at 750 °C. In-between the exposures, the quartz tube was cleaned by an empty run with a chromium getter material.

The cells after exposure were tested electrically for their in fuel cell/electrolysis performance. For electrochemical performance, a Fiaxell Open Flange V5 test Set-up developed (Fiaxel Sarl, Lausanne, Switzerland) was used. A top side of the oxygen electrode was painted with $La_{0.6}Sr_{0.4}CoO_3$ (Fiaxell, Lausanne, Switzerland) contact paste and dried before installation in the measurement setup. The electrical connection with a cell was provided by a gold grid from a cathode side and a Ni mesh on the anode side. The Au wires were connected to a Solartron 1260/1287 (Solartron Analytical, Leicester, UK) system for impedance and current-voltage characterization. Both electrodes have been separated by alumina felt and working gases were directly supplied to the individual electrodes by ceramic tubes, i.e. avoiding any extra Cr poisoning source. The gas flows were controlled by mass flow controllers (Alicat Scientific, Tucson, AZ, USA). After heating to 750 °C, the reduction of the cell occurred in dry H_2 until a stable OCV value (~1.1 V) was obtained. For cell performance characterization, current-voltage (I-V) characteristics and

electrochemical impedance spectroscopy (EIS) were measured. The cells were examined in fuel cell mode using humidified H_2 as a fuel and also measured under 50% H_2O – 50% H_2 gas mixture for characterization in the electrolysis mode.

2.4 Morphological and compositional characterization

Morphological and compositional characterization of both as-prepared and post-mortem samples was carried out by a scanning electron microscope (SEM, Zeiss Supra) equipped with an energy dispersive X-Ray analyser (EDX, Bruker). To examine the cross sections, samples were embedded in epoxy resin and polished up to 4000 SiC paper. The coatings porosity was evaluated by a graphical method using the IMAGEJ software [33], analyzing three SEM images from different regions of each sample.

3. Results and discussion

3.1. Characterization of as-prepared samples

Figure 1 a-b shows SEM images of the cross section of the coating submitted to the one-step sintering. The coating is continuous throughout the sample surface, with a thickness ranging from around 16 to 17 µm. It is apparent from this image that the densification obtained after the oxidation treatment is poor, as confirmed by the calculated mean porosity, that exceeds 50%. However, the coating is very homogeneous, with the porosity equally distributed over the whole thickness. It is evident that the coating adheres to the Crofer 22 APU substrate very well and that there are no visible delamination phenomena or cracks at the coating/Crofer 22 APU interface.

The oxide scale developed during the heat treatment is visible as the darker layer between steel substrate and the coating in Figure 1 b. The irregular and jagged morphology prevents to accurately assess the thickness, which was found to be between 0.3 and 0.8 µm, in reasonable agreement with other studies [21,29]. EDX analysis of marked areas in Figure 1 a demonstrates that Cr concentration in the coating is almost negligible, despite being higher in the inner part.

SEM images of the top view of the 20s_Ox sample are reported in Figure 1 c-d; the MCO particles are still clearly distinguishable, proving that the heat treatment in air at 900 °C led to limited densification.

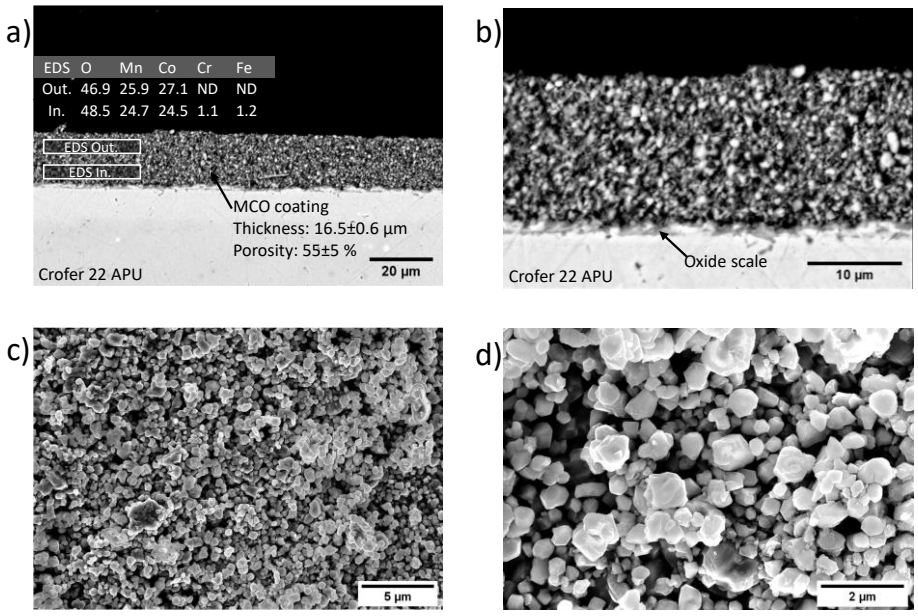

Figure 1. SEM images of 20s_Ox sample at different magnifications: (a,b) back scattered electrons images and EDX analysis of the cross section; (c,d) secondary electrons images of the top view.

The SEM cross sections and top view images of 20s_Red coating and the related EDS elemental maps are shown in Figure 2 a-d. In this case, the heat treatment in reducing atmosphere at 1000 °C led to a higher coating densification. However, residual porosity is still significant (approximately 35 %). The performed heat treatment in reducing atmosphere has already been proved to effectively cause the MCO powder to decompose into MnO and Co [25,34]. This is confirmed with EDX area analysis reported in Figure 2 a, as cobalt relative amount increases significantly. In particular, metallic cobalt particles correspond to the brightest spots in Figure 2 b.

The oxide scale is regular and presents good adhesion to the coating, thanks to the high temperature treatment. Although the measured thicknesses lay in the same range as the 20s_Ox sample, the morphology of the chromia layer is very different among the two cases. Indeed, 20s_Red exhibits a compact layer, without inward protrusion in the steel (as observed in Figure 1 b instead). Moreover, the Cr content in the coating is negligible both in the inner and out part (Figure 2 a).

The SEM top views of 20s_Red in Figure 2 c-d reveal that the reduction was effective in producing partially densified structures and the coating lost the appearance of packed particles, compared to 20s_Ox sample. However, quite large porosities (≈ 1-2μm) are present on the surface of the sample.

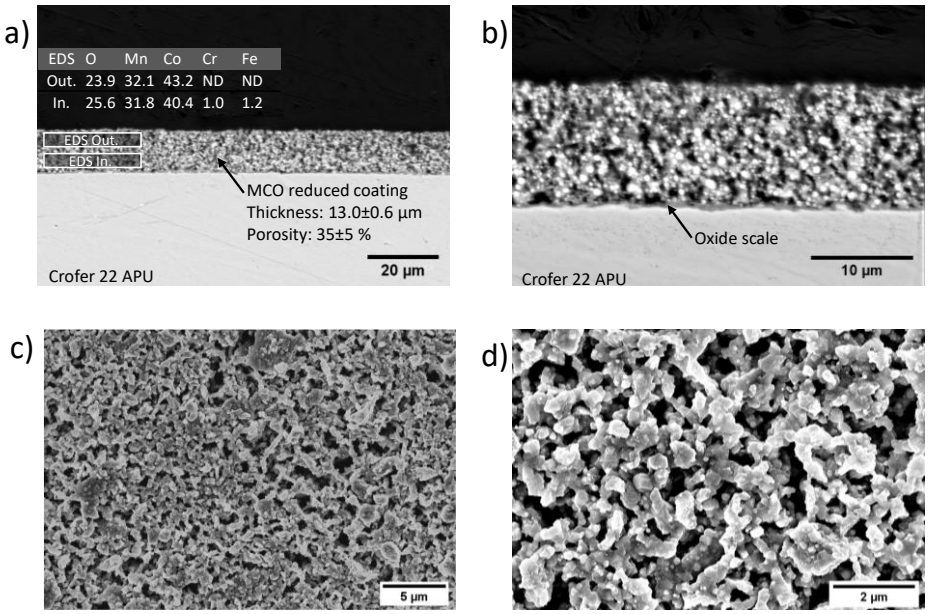

Figure 2. SEM images of 20s_Red sample at different magnifications: (a, b) back scattered electrons images and EDX analysis of the cross section; (c, d) secondary electrons images of the top view.

More interesting features can be appreciated by comparing SEM images previously described of 20s_Ox and 20s_Red with those of the coating after the re-oxidation step (20s_RedOx), thus at the end of the two-step sintering; the SEM cross sections and top view images are presented in Figure 3 a-d. During the re-oxidation step, MnO and Co are supposed to react in order to re-form the spinel structure but bringing benefit in terms of densification [20]. To this purpose, the most evident characteristic is the significant densification (80 %) reached after the re-oxidation step, with a final coating thickness of around 12 μm. Moreover, it is worth to note that the residual porosity is not homogeneously distributed throughout the coating. Indeed, a denser layer is easily distinguishable in the inner part of the 20s_RedOx coating (Figure 3 b). This layer uniformly covers the oxide scale, thus protecting the steel from direct contact with air during operation of the device. Therefore, most of the porosity is concentrated in the outer part of the coating. Furthermore, the thickness of the oxide scale is very similar to the one measured after the reduction, even if few and small sub-scale nodules are distinguishable: they are formed because of the reaction of Cr, Mn and O in oxidizing condition at high temperature [26]; however,

their growth should be limited during long-term aging, thanks to the healing effect of the coating which is completed after re-oxidation [25].

EDX analysis reported in Figure 3 a do not show any significant difference from what was already commented for the previous samples, proving that the improved densification is not the consequent of any abnormal diffusion of neither Cr nor Fe from the steel during the heat treatment. Apparently, metallic cobalt diffusion during the re-oxidation was very beneficial to densify the partially sintered structures already visible in Figure 2 c-d, closing or at least reducing the dimension of the porosity on the surface of the coating. The difference with the images presented in Figure 1 c-d is obvious; here the coating has completely lost the appearance of particles and the densified structures clearly exhibit the typical microstructure of the Mn-Co spinel.

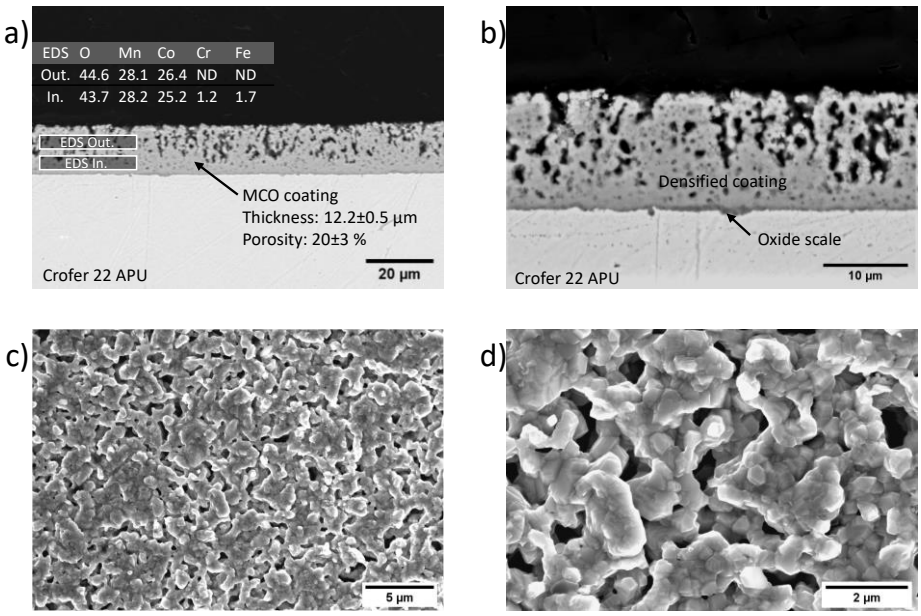

Figure 3. SEM images of 20s_RedOx sample at different magnifications: (a, b) back scattered electrons images and EDX analysis of the cross section; (c, d) secondary electrons images of the top view.

To examine how the sintering process and coating density affect the electrical properties of the samples, ASR values of the coated coupons were measured. The temperature dependence of the ASR is shown in Figure 4 b. At 750 °C, the measured values are ~7.2 mΩ cm² and ~7.9 mΩ cm² for 20s_RedOx and 20s_Ox sample, respectively. As the temperature decreases, the difference in resistance increases: at 500 °C the ASR measured for the 20s_RedOx sample is half that of the 20s_Ox sample (~40 mΩ cm²); at the lowest tested temperature ASR for 20s_Ox sample is ~5 times higher than for 20s_RedOX sample (~35 Ω cm²). The differences in these values are due to the different porosity of the deposited coatings and different thickness of the oxide scale.

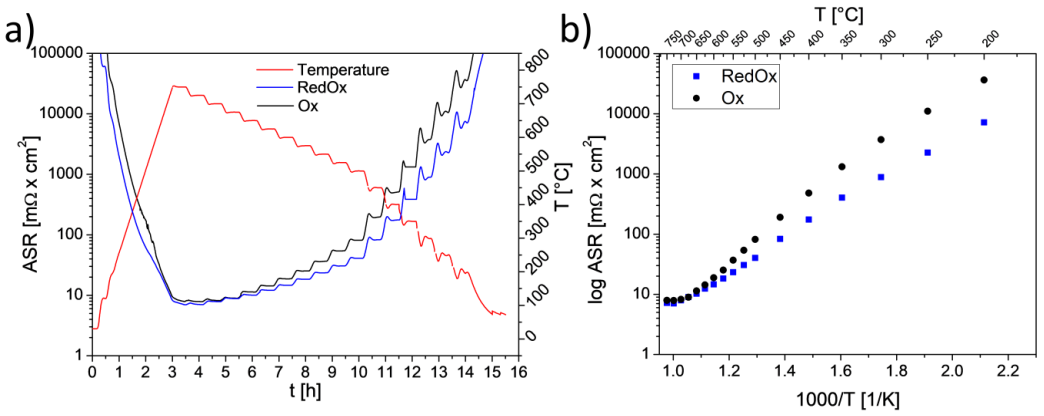

Figure 4. ASR measurement of the as-prepared 20s_Ox and 20s_RedOx samples: (a) as a function of time; (b) as a function of temperature.

3.2. Aging exposure at 750 °C and cell test results

To evaluate the protective properties of prepared coatings, the electrochemical behavior of aged ASC-SOFCs was determined using I-V and EIS characterization. Figure 5 summarizes current voltage (I-V), power density (PD) curves and impedance spectroscopy (EIS) results obtained at 750 °C under continuous flow of synthetic air as oxidant and humidified hydrogen as fuel. The cells achieved OCV of 1.07 V, and 1.09 V for reference and both interconnect-exposed cells, respectively. As it can be seen, I-V curves and the maximum power densities were comparable for cells exposed with 20s_RedOx and 20s_Ox interconnects, i. e. achieved P_{max} ~0.71-0.72 W/cm², which is a typical performance of these cells. The minor difference was observed for the reference sample showed P_{max} ~ 0.68 W/cm². A similar observation was for cells operated in the electrolysis mode under 50%H_2O -50%H_2 as a fuel. The slope of all I-V curves was identical for voltages below OCV with an 0.02V offset of the reference sample, possibly due to small leaks. Under applied current load, the cell exposed with the 20s_RedOx sample presents a slightly better electrolysis performance.

The EIS measurement allowed to determine polarization and ohmic resistances (R_{pol} and R_{ohm}) at OCV and corresponding Bode and Nyquist plots are shown in Figure 4 b and 4 c. For the cells working under humidified H_2 as a fuel, the resistance values of the cells were similar. The cell exposed with 20s_RedOx sample had R_{ohm} = 0.23 Ω·cm², R_{pol} = 0.38 Ω·cm², the cell with 20s_Ox sample had R_{ohm} = 0.22 Ω·cm² and R_{pol} = 0.40 Ω·cm², and the reference sample had R_{ohm} = 0.24 Ω·cm² and R_{pol} = 0.39 Ω·cm². There are no significant differences in resistances of compared cells in fuel cell mode. The situation is slightly different in the case of cells tested in the electrolyzer mode. While the reference cell and cell aged with the sample 20s_RedOx have the same resistances of R_{ohm} = 0.24 Ω·cm² and R_{pol} = ~0.17 Ω·cm² values, the aged cell with 20s_Ox coating shows slightly different values of R_{ohm} = 0.20 Ω·cm² and R_{pol} = 0.20 Ω·cm². The minor differences are more likely attributed to the reproducibility issues than to the effect of Cr evaporation and performance degradation.

Interestingly, both the porous (20s_Ox) and dense (20s_RedOx) coatings are able to protect the cell from reaction with Cr-vapors, in contrast with the work by Abdoli et al. [21]. In our case the study was performed at lower temperature (250 h at 750 °C instead of 100 h at 800 °C) and the cathode material was LSCF, whereas in [21] it was LSM. Also, the microstructure of the spinel coating differs: Abdoli et al. have used a thinner coating (≤5 μm), which can result in different evaporation rates.

To explain the protective behavious of the 20s_Ox and 20s_RedOx coatings, microstructural characterization of cells and interconnects was performed.

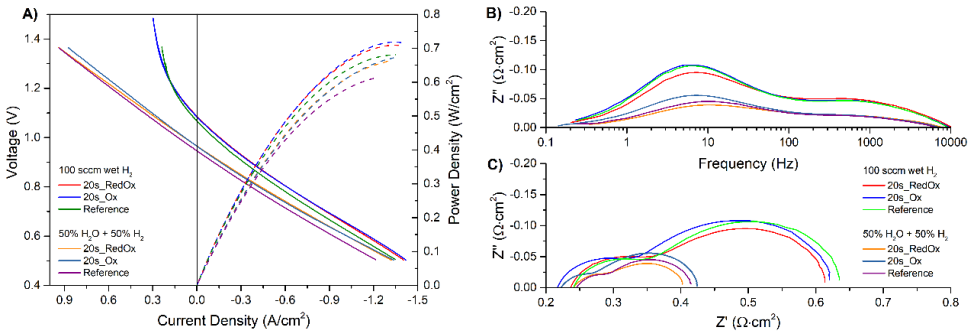

Figure 5. Plots of the examined cells measured at 750°C: (a) I-V curves; (b) Bode plot; (c) Nyquist plot.

3.3. Post-mortem characterization

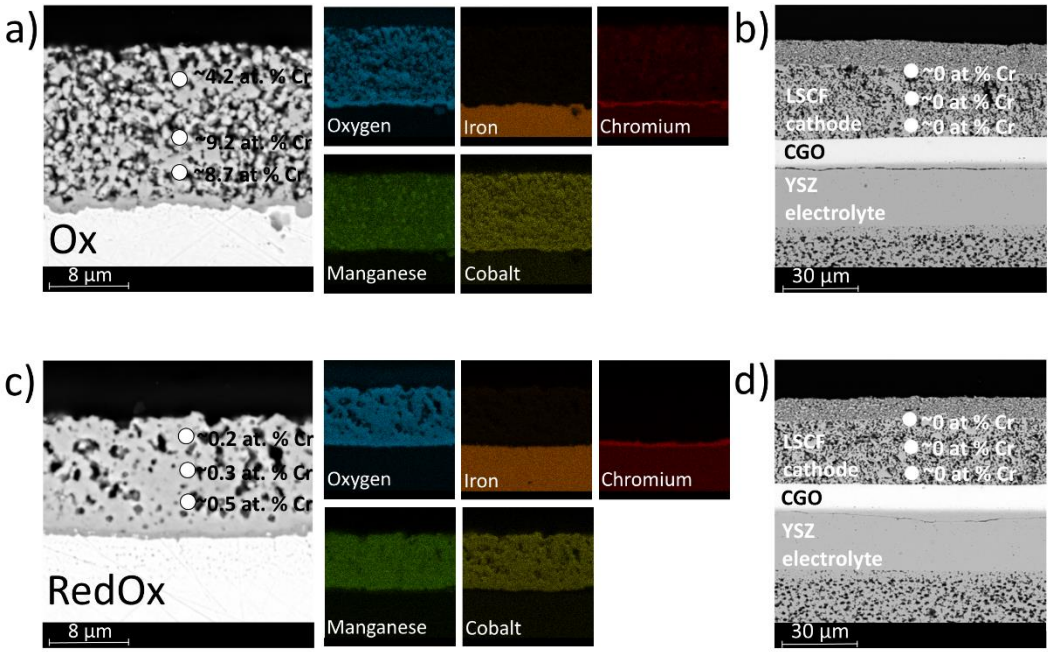

Figure 6. Post-mortem SEM analysis: (a) 20s_Ox sample; (b) fuel cell exposed with 20s_Ox sample; (c) 20s_RedOx sample; (d) fuel cell exposed with 20s_RedOx sample.

The microstructures and chemical compositions (elemental distribution) of the coatings after 250 h of oxidation at 750 °C in humidified air flow are shown in Figure 6 a and Figure 6 c. Comparing the chromium distribution, large differences can be observed between the samples. For the two-step sintered 20s_RedOx sample, chromium occurs only at the steel-coating interface, i.e. forming chromium oxide scale. In the sample sintered only in air - 20s_Ox, the chromium is present in the whole coating. According to the quantitative EDX point analysis the amount of Cr in the 20s_RedOx sample varies from 0.5 at.% to 0.2 at.% above the chromium oxide layers and on top of the coating, respectively. For the sample with higher porosity (20s_Ox), the chromium content is from 4-7 at.%, without following a concentration gradient from the steel to the top on the coating.

In addition, for the 20s_RedOx coating, the manganese to cobalt ratio is as expected (to a very good approximation 1:1), consistent with the stoichiometry of the raw spinel powder. The manganese content of the coating sintered in air – 20s_Ox is higher than that of the starting powder, as the manganese to cobalt ratio is 1.13: 1 (average obtained from 5 point EDX analyses), indicating Mn enrichment. This observation can indicate that high

density coating slows down both chromium and managnese diffusion from the ferritic steel substrate.

To identify if any chromium species can be found in the cathode, the same EDX analyses procedures as for the coatings was performed. SEM images and point EDX analysis are presented in Figure 6 b and Figure 6 d. Point analysis of the LSCF cathode composition showed no chromium in either the 20s_RedOx or the 20s_Ox sample, consistent with the electrochemical results. The analysis of the EDX spectrum for LSC is of difficult interpretation due to the overlap of the chromium and lanthanum peaks, but the qualitative comparison of La and Cr signals does not indicate Cr diffusion.

The study reveals that even the higly porous spinel coating reduced the Cr poisoning of the LSCF oxygen electrode. Though the porous coating is much more reactive than the dense one, for the relatively short test time and moderate temperature considered in this study, it seems as a viable protective solution. In the porous 20s_Ox coating, the Mn-Co spinel reacts with the diffusing Cr and Mn forming a mixed spinel, which must have relatively low Cr-evaporation rate, and acts as a Cr-getter material in this case.

4. Conclusions

High quality manganese-cobalt spinel coatings prepared by electrophoretic deposition were evaluated for their potential to block Cr-evaporation and poisoning of LSCF oxygen electrodes. Two different microstructures, including porous air-only and dense, redox sintered samples, showed noticeable differences in Cr retention capability. Interestingly, both of the coatings were shown to block Cr-evaporation and cell poisoning, as determined by similar electrochemical performance (power density, ohmic and polarization resistance) of the cells after the aging exposures. However, microstructural studies revealed large differences between the samples: the porous coating reacted with Cr and Mn diffusing from the Crofer 22 APU steel/oxide whereas the dense 20s_RedOx coating remained mostly unchanged and virtually Cr-free. The porous spinel acted as a Cr-getter material, binding Cr-species and limiting further evaporation and cell degradation. The results show that the microstructure of the manganese cobalt coatings has a large effect on their protective performance and determines the possible mechanisms of degradation.

Author Contributions: For research articles with several authors, a short paragraph specifying their individual contributions must be provided. The following statements should be used "Conceptualization, F. S.. E. Z. and S. M..; methodology, E. Z., B. K., J. I.; investigation, E. Z., B. K, J. I.; resources, F.S. S. M.; data curation, B.K.; writing—original draft preparation, E.Z.; writing—review and editing, F. S. A. R. B. S. M.; supervision, F. S., S. M. and A. R. B.; project administration, F.S.; funding acquisition, S.M, P. J. All authors have read and agreed to the published version of the manuscript." Please turn to the CRediT taxonomy for the term explanation. Authorship must be limited to those who have contributed substantially to the work reported.

Funding: "This research was funded by by National Science Centre (NCN) Harmonia 9 project number UMO-2017/26/M/ST8/00438: "Quest for novel materials for solid oxide cell interconnect coatings". Funding of WETI PG is also gratefully acknowledged.

Conflicts of Interest: the authors declare no conflict of interest. Declare conflicts of interest or state "The authors declare no conflict of interest." Authors must identify and declare any personal circumstances or interest that may be perceived as inappropriately influencing the representation or interpretation of reported research results. Any role of the funders in the design of the study; in the collection, analyses or interpretation of data; in the writing of the manuscript, or in the decision to publish the results must be declared in this section. If there is no role, please state "The funders had no role in the design of the study; in the collection, analyses, or interpretation of data; in the writing of the manuscript, or in the decision to publish the results".

References

1. Stanislowski, M.; Wessel, E.; Hilpert, K.; Markus, T.; Singheiser, L. Chromium Vaporization from High-Temperature Alloys. *J.*

Electrochem. Soc. **2007**, *154*, A295.

2. Shaigan, N.; Qu, W.; Ivey, D.G.; Chen, W. A review of recent progress in coatings, surface modifications and alloy developments for solid oxide fuel cell ferritic stainless steel interconnects. *J. Power Sources* **2010**, *195*, 1529–1542.
3. Mah, J.C.W.; Muchtar, A.; Somalu, M.R.; Ghazali, M.J. Metallic interconnects for solid oxide fuel cell: A review on protective coating and deposition techniques. *Int. J. Hydrogen Energy* **2017**, *42*, 9219–9229.
4. Tan, K.H.; Rahman, H.A.; Taib, H. Coating layer and influence of transition metal for ferritic stainless steel interconnector solid oxide fuel cell: A review. *Int. J. Hydrogen Energy* **2019**, *44*, 30591–30605, doi:10.1016/j.ijhydene.2019.06.155.
5. Masi, A.; Bellusci, M.; McPhail, S.J.; Padella, F.; Reale, P.; Hong, J.-E.; Steinberger-Wilckens, R.; Carlini, M. The effect of chemical composition on high temperature behaviour of Fe and Cu doped Mn-Co spinels. *Ceram. Int.* **2016**, *43*, 2829–2835.
6. Talic, B.; Molin, S.; Wiik, K.; Hendriksen, P.V.; Lein, H.L. Comparison of iron and copper doped manganese cobalt spinel oxides as protective coatings for solid oxide fuel cell interconnects. *J. Power Sources* **2017**, *372*, 145–156.
7. Molin, S.; Sabato, A.G.; Javed, H.; Cempura, G.; Boccaccini, A.R.; Smeacetto, F. Co-deposition of CuO and Mn1.5Co1.5O4 powders on Crofer22APU by electrophoretic method: Structural, compositional modifications and corrosion properties. *Mater. Lett.* **2018**, *218*, 329–333, doi:10.1016/j.matlet.2018.02.037.
8. Zhu, J.H.; Lewis, M.J.; Du, S.W.; Li, Y.T. CeO2-doped (Co, Mn)3O4 coatings for protecting solid oxide fuel cell interconnect alloys. *Thin Solid Films* **2015**, *596*, 179–184, doi:10.1016/j.tsf.2015.07.085.
9. Brylewski, T.; Molin, S.; Marczyński, M.; Mazur; Domaradzki, K.; Kryshtal, O.; Gil, A. Influence of Gd deposition on the oxidation behavior and electrical properties of a layered system consisting of Crofer 22 APU and MnCo2O4 spinel. *Int. J. Hydrogen Energy* **2021**, *46*, 6775–6791, doi:10.1016/j.ijhydene.2020.11.169.
10. Mosavi, A.; Ebrahimifar, H. Investigation of oxidation and electrical behavior of AISI 430 steel coated with Mn–Co–CeO2 composite. *Int. J. Hydrogen Energy* **2020**, *45*, 3145–3162, doi:10.1016/j.ijhydene.2019.11.183.
11. Stanislowski, M.; Froitzheim, J.; Niewolak, L.; Quadakkers, W.J.; Hilpert, K.; Markus, T.; Singheiser, L. Reduction of chromium vaporization from SOFC interconnectors by highly effective coatings. *J. Power Sources* **2007**, *164*, 578–589.
12. Molin, S.; Sabato, A.G.; Bindi, M.; Leone, P.; Cempura, G.; Salvo, M.; Cabanas Polo, S.; Boccaccini, A.R.; Smeacetto, F. Microstructural and electrical characterization of Mn-Co spinel protective coatings for solid oxide cell interconnects. *J. Eur. Ceram. Soc.* **2017**, *37*, 4781–4791.
13. Bateni, M.R.; Wei, P.; Deng, X.; Petric, A. Spinel coatings for UNS 430 stainless steel interconnects. *Surf. Coatings Technol.* **2007**, *201*, 4677–4684, doi:10.1016/j.surfcoat.2006.10.011.
14. Han, S.J.; Pala, Z.; Sampath, S. Plasma sprayed manganese–cobalt spinel coatings: Process sensitivity on phase, electrical and protective performance. *J. Power Sources* **2016**, *304*, 234–243.
15. Lee, S.-I.; Hong, J.; Kim, H.; Son, J.-W.; Lee, J.-H.; Kim, B.-K.; Lee, H.-W.; Yoon, K.J. Highly Dense Mn-Co Spinel Coating for Protection of Metallic Interconnect of Solid Oxide Fuel Cells. *J. Electrochem. Soc.* **2014**, *161*, F1389–F1394.
16. Kruk, A.; Stygar, M.; Brylewski, T. Mn–Co spinel protective–conductive coating on AL453 ferritic stainless steel for IT-SOFC interconnect applications. *J. Solid State Electrochem.* **2013**, *17*, 993–1003.
17. Xiao, J.; Zhang, W.; Xiong, C.; Chi, B.; Pu, J.; Jian, L. Oxidation behavior of Cu-doped MnCo2O4 spinel coating on ferritic stainless steels for solid oxide fuel cell interconnects. *Int. J. Hydrogen Energy* **2016**, *41*, 9611–9618.
18. Shen, Z.; Rong, J.; Yu, X. MnxCo3-xO4 spinel coatings: Controlled synthesis and high temperature oxidation resistance behavior. *Ceram. Int.* **2020**, *46*, 5821–5827, doi:10.1016/j.ceramint.2019.11.032.
19. Hu, S.; Li, W.; Finklea, H.; Liu, X. A review of electrophoretic deposition of metal oxides and its application in solid oxide fuel cells. *Adv. Colloid Interface Sci.* **2020**, *276*, 102102, doi:10.1016/j.cis.2020.102102.
20. Zanchi, E.; Sabato, A.G.; Molin, S.; Cempura, G.; Boccaccini, A.R.; Smeacetto, F. Recent advances on spinel-based protective coatings for solid oxide cell metallic interconnects produced by electrophoretic deposition. *Mater. Lett.* **2021**, *286*, 129229, doi:10.1016/j.matlet.2020.129229.

21. Abdoli, H.; Molin, S.; Farnoush, H. Effect of interconnect coating procedure on solid oxide fuel cell performance. *Mater. Lett.* **2020**, *259*, 126898, doi:10.1016/j.matlet.2019.126898.
22. Kalinina, E.G.; Pikalova, E.Y. New trends in the development of the method of electrophoretic deposition in the SOFC technology: theoretical approaches, experimental solutions and development perspectives. *Russ. Chem. Rev.* **2019**, *88*, doi:10.1070/rcr4889.
23. Besra, L.; Liu, M. A review on fundamentals and applications of electrophoretic deposition (EPD). *Prog. Mater. Sci.* **2007**, *52*, 1–61.
24. Talic, B.; Wulff, A.C.; Molin, S.; Andersen, K.B.; Zielke, P.; Frandsen, H.L. Investigation of electrophoretic deposition as a method for coating complex shaped steel parts in solid oxide cell stacks. *Surf. Coatings Technol.* **2019**, *380*, 1–8, doi:10.1016/j.surfcoat.2019.125093.
25. Zanchi, E.; Talic, B.; Sabato, A.G.; Molin, S.; Boccaccini, A.R.; Smeacetto, F. Electrophoretic co-deposition of Fe2O3 and Mn1,5Co1,5O4: Processing and oxidation performance of Fe-doped Mn-Co coatings for solid oxide cell interconnects. *J. Eur. Ceram. Soc.* **2019**, *39*, 3768–3777, doi:10.1016/j.jeurceramsoc.2019.05.024.
26. Zanchi, E.; Molin, S.; Sabato, A.G.; Talic, B.; Cempura, G.; Boccaccini, A.R.; Smeacetto, F. Iron doped manganese cobaltite spinel coatings produced by electrophoretic co-deposition on interconnects for solid oxide cells: Microstructural and electrical characterization. *J. Power Sources* **2020**, *455*, 227910, doi:10.1016/j.jpowsour.2020.227910.
27. Sabato, A.G.; Molin, S.; Javed, H.; Zanchi, E.; Boccaccini, A.R.; Smeacetto, F. In-situ Cu-doped MnCo-spinel coatings for solid oxide cell interconnects processed by electrophoretic deposition. *Ceram. Int.* **2019**, *45*, 19148–19157.
28. Sabato, A.G.; Zanchi, E.; Molin, S.; Cempura, G.; Javed, H.; Herbrig, K.; Walter, C.; Boccaccini, A.R.; Smeacetto, F. Mn-Co spinel coatings on Crofer 22 APU by electrophoretic deposition: Up scaling, performance in SOFC stack at 850 °C and compositional modifications. *J. Eur. Ceram. Soc.* **2021**, *41*, 4496–4504, doi:10.1016/j.jeurceramsoc.2021.03.030.
29. Bobruk, M.; Molin, S.; Chen, M.; Brylewski, T.; Hendriksen, P.V. Sintering of MnCo2O4 coatings prepared by electrophoretic deposition. *Mater. Lett.* **2018**, *213*, 394–398, doi:10.1016/j.matlet.2017.12.046.
30. Talic, B.; Falk-Windisch, H.; Venkatachalam, V.; Hendriksen, P.V.; Wiik, K.; Lein, H.L. Effect of coating density on oxidation resistance and Cr vaporization from solid oxide fuel cell interconnects. *J. Power Sources* **2017**, *354*, 57–67.
31. Falk-Windisch, H.; Svensson, J.E.; Froitzheim, J. The effect of temperature on chromium vaporization and oxide scale growth on interconnect steels for Solid Oxide Fuel Cells. *J. Power Sources* **2015**, *287*, 25–35, doi:10.1016/j.jpowsour.2015.04.040.
32. Smeacetto, F.; De Miranda, A.; Cabanas Polo, S.; Molin, S.; Boccaccini, D.; Salvo, M.; Boccaccini, A.R. Electrophoretic deposition of Mn1.5Co1.5O4 on metallic interconnect and interaction with glass-ceramic sealant for solid oxide fuel cells application. *J. Power Sources* **2015**, *280*, 379–386, doi:10.1016/j.jpowsour.2015.01.120.
33. Schneider, C.A.; Rasband, W.S.; Eliceiri, K.W. NIH Image to ImageJ: 25 years of image analysis. *Nat. Methods* **2012**, *9*, 671–675.